VER
Vascular & Endovascular Review

Synergistic Anticancer Potential of Probiotics and Curcumin-Loaded Chitosan Nanoparticles against Colorectal Cancer

Dr Ankur Singh[1], Dr Vishwa Joshi[2], Abhishek Anand[3], Mansi Sharma[4], Sambit Kumar Parida[5], Dr Mohammad Farooque[6]*

[1]Associate Professor, Sahu Onkar Saran School of Pharmacy, Faculty of Pharmacy, IFTM University, Moradabad, U.P., Pincode: 2244102
[2]PG Final year Student, Parul Institute of Ayurved, Parul University P.O. Limda Tal. Waghodia Dist. Vadodara – 391760 Gujarat State, India
[3]Assistant Professor, Department of Pharmacy practice, Teerthanker Mahaveer College of Pharmacy, Teerthanker Mahaveer University Moradabad, 244001
[4]Assistant Professor, Department of Pharmacy, IBMER, Mangalayatan University, Aligarh
[5]Professor & Director, Amity Institute of Pharmacy, Amity University Rajasthan, India-303002
*[6]Assistant Professor, SBKS MIRC, Sumandeep Vidyapeeth, Pipariya – 391760
Corresponding Author: Dr Mohammad Farooque
Email: ankursingh108@gmail.com, vishwaa97826@gmail.com, abhishekanandabhi66@gmail.com, mansi.sharma@mangalayatan.edu.in, dr.sambit@yahoo.com, mfarooque6@gmail.com

ABSTRACT

Colorectal cancer (CRC) is among the leading causes of cancer related mortality among populations in the world. Despite the mentioned progress in the traditional treatments e.g. chemotherapy, it has shown minimal efficacy due to the development of drug resistance and other serious side effects and of different lacks good targeting. The article discusses the synergistic anticancer activity of chitosan nanoparticle (NPs) loaded with probiotics and curcumin in the treatment of CRC. Curcumin is a natural bioactive compound with immense anticancer characteristics, nevertheless, curcumin possesses low bioavailability and low solubility. To counter such a limitation, curcumin is encased in chitosan-based nanoparticles, which, in addition, provides a controlled release of drugs and enhances its stability. There is also the addition of probiotics, which are attributed with their ability to balance the bioflora of the gut and improving the immune functionality, in order to increase the therapeutic effect of curcumin. In the paper, the cytotoxicity, drug delivery, and combinatorial anticancer studies of chitosan nanoparticles loaded with curcumin have been reported in vitro and in vivo using colorectal cells (HT-29) under cancer research. The results reveal that the anticancer potential of curcumin loaded nanoparticles with probiotics enhances significantly the effect of the former by modifying the tumor microenvironment and improving the bioavailability of the drug. This implies that the combination therapy was not only more efficient but also minimized systemic toxicity too hence the application of nanomedicine combination method of curcumin to be very effective in cancer therapy of the colorectal cancer.

KEYWORDS: Colorectal cancer, Probiotics, Curcumin, Chitosan nanoparticles, Nanomedicine, Anticancer therapy, Drug delivery, Synergistic effects.

How to Cite: Faris Ankur Singh, Vishwa Joshi, Abhishek Anand, Mansi Sharma, Sambit Kumar Parida, Mohammad Farooque., (2025) Synergistic Anticancer Potential of Probiotics and Curcumin-Loaded Chitosan Nanoparticles against Colorectal Cancer, Vascular and Endovascular Review, Vol.8, No.10s, 94--114.

INTRODUCTION

Colorectal cancer (CRC) has a very wide distribution with the risk probability of all the available cancer diseases in the globe with a probability of approximately 10 percent of the total and 9.2 percent of the total cancer-induced deaths. It is a serious health problem of the community which is extremely widespread, especially, in developed societies [1]. CRC is primarily started in the colon or inside the rectum and more frequently than not, it starts as benign polyps which eventually underdevelop into cancerous cells with time having not been established. CRC risk factors can be characterized as multifactorial because they include a genetic predisposition, lifestyle-related (e.g., diet, physical inactivity, and alcohol consumption), chronic inflammatory disease, and age [2]. Nonetheless, the survival of patients with advanced or metastatic CRC after surgery, chemotherapy, and radiotherapy remains poor even after the method of surgery was developed. The current treatment procedures are commonly known to have severe side effects, less effectiveness on tumors during the later stage and relapses, thus it is highly imperative to come up with new and effective treatment means [3]. Chemotherapy where cytotoxic agents are administered to kill the rapidly growing cancerous cells is the primary mode of management of the CRC condition [4]. However, these agents are usually unselective in nature and lead to systemic toxicity and damage of normal tissues particularly in vital organ, liver, kidney as well as bone marrow. Amongst the many used chemotherapeutic drugs in management of CRC, 5-Fluorouracil (5-FU), 5-FU is a pyrimidine analog which inhibits the DNA synthesis of cancer cells [5]. However, its clinical use is restricted by the unwanted side effects which include myelosuppression, gastrointestinal and neurotoxicity. Also, due to the prolonged effects, 5-FU can result in resistance which complicates the treatment outcome even more [6]. Therefore, there exist an up-to-date tendency to explore other or alternative therapies capable of enhancing the treatment efficacy of the conventional treatment and minimizing its side effects and resistance to drugs in CRC [7].

Another sector of nanomedicine whose foundation lies with the use of nanotechnology material is the development of better drug delivery devices. Other advantages of using nanoparticles in cancer therapy include improved solubility of drugs, controlled release, targeting and bioactive barriers, including the blood-brain barrier or extracellular matrix [8]. In particular, nanoparticles can be programmed, so that they may be loaded with a chemotherapeutic species, and thus, to be less toxic to normal cells, and tighter concentrated at the site of the abnormal growth. Many nanoparticles have been fabricated to treat cancer like liposomal nanoparticles, polymeric nanoparticles and the chitosan-based nanoparticles [9]. Chitosan is a natural polysaccharide which is chitin and has enormous applications in biomedical field, including its biocompatibility, biodegradability and ability to modify drug delivery properties. This has seen it readily react with negatively charges molecules like medications and DNA since it is cationic in character and it is therefore good candidate in nanoparticle based drug delivery systems [10]. Curcumin, one of the active compounds of the turmeric plant (Curcuma longa) has proven to exhibit good anticancer activity through diverse different approaches, including inhibition of tumor growth, induction of cell death (apoptosis), and inhibition of inflammation [11]. The research has also shown that curcumin has the ability to control numerous significant cancer-related signaling pathways which include the NF- -B, the MAPK and the PI3K/Akt pathways. These properties have however limited its clinical use due to its low solubility in water, high metabolism rate, in addition to its low bioavailability [12]. In order to overcome these disadvantages, curcumin has been loaded in many nanoparticles like chitosan systems to increase the solubility of curcumin, stability and localization of curcumin to the cancer cells. This enhances its cancer effects as well as off-target toxicity. Probiotics have been mentioned too as dietary supplement in cancer treatment besides curcumin, due to their proficiency in controlling the gut microbiota, boosting the immune response and having a direct influence on tumor growth [13]. Certain probiotics, specially Lactobacillus and Bifidobacterium probiotics, were also discovered to exhibit anticancer activity as being synonymous in disrupting inflammatory reactions, apoptosis and in reducing oxidative stress. Other than that, probiotics could also promote bioavailability and pharmacologic responses of encapsulated medications, e.g., curcumin, by boosting drug absorption and drug retention in the gastrointestinal tract [14].

The combination of the probiotics with curcumin and nanoparticles suggests a new strategy to facilitating the treatment effectiveness of the curing of CRC [15]. The logic behind this combination is that the three elements possess synergistic capability against the cancer cells. With nanoparticles loaded with curcumin, delivery of the drug to the tumor site in a targeted and regulated manner will be achievable, which will increase its anticancer effect and decreases the toxicity at the system-wide level [16]. On the other hand, Probiotics can also help to enhance the immune system, maintain gut microorganisms and also maintain the stability and bioavailability of the nanoparticles that are loaded with curcumin. Along with this, probiotics have also been proven to be directly interacting with nanoparticles, encouraging the release of drugs and the stability of nanoparticle formulation in general [17]. Such is a synergistic idea that can result in a more effective treatment plan that can be used to contextualize the tumour and the microenvironment behind it and amplify the effect of anticancer whilst reducing adverse effects [18]. The use of such research findings can be harnessed in immeasurable ways to devise new and more effective curative procedures to cancer. This type of a combination of therapeutic qualities of curcumin, probiotics, and nanoparticles composed of chitosan can be used as a more directed and less toxic alternative to the traditional chemo-therapy. In addition, the integration of probiotics and curcumin loaded nanoparticle could offer an alternative that can enhance bioavailability and therapeutic effect of curcumin that has tremendous potential and poor clinical utility. These results could result in the creation of multifunctional systems of nanoparticles, which can hit on the cancer cells and the tumor microenvironment at the same time and will have the ability of offering a more complete and more effective approach to cancer treatment of colorectal cancer.

METHODS AND MATERIALS

2.1 Materials

Chitosan (CS), curcumin, 5-Fluorouracil (5-FU), tripolyphosphate (TPP), sodium hydroxide (NaOH), and other chemicals were sourced from reputable suppliers (Sigma-Aldrich, Merck, etc.). The probiotic strains, Lactobacillus spp., were obtained from culture collections and maintained according to standard protocols.

2.2 Synthesis of N, O-Carboxymethyl Chitosan (N, O-CMC)

N, O-CMC was synthesized through a carboxymethylation reaction of chitosan with chloroacetic acid in an alkaline medium. The reaction mechanism involves the reaction of chitosan's -OH groups with NaOH to form sodium methoxide, which then reacts with chloroacetic acid. This results in the O-carboxymethylation. The -NH2 groups of chitosan undergo carboxymethylation in the second step at 60°C for 3 hours, forming N-carboxymethyl chitosan. The degree of carboxymethyl substitution was determined using the titrimetric method, and the water solubility of N, O-CMC was confirmed through solubility tests. The product was characterized by FT-IR to confirm the functional group modifications.

2.3 Preparation of N, O-CMC Nanoparticles (NPs)

N, O-CMC nanoparticles were prepared by ionic gelation using TPP. The protonated amine groups of N, O-CMC interact with the negatively charged phosphate groups of TPP to form nanoparticles. The size and surface charge of the nanoparticles were characterized using Dynamic Light Scattering (DLS), Scanning Electron Microscopy (SEM), and Atomic Force Microscopy (AFM). Zeta potential measurements were conducted to assess the stability of the nanoparticles.

2.4 Preparation of Thiolated Chitosan (TCS)

TCS was synthesized by reacting chitosan with thioglycolic acid (TGA) using carbodiimide chemistry (EDC-catalyzed reaction). The formation of the amide bond was confirmed by FT-IR spectroscopy, and the degree of thiol substitution was quantified using Ellman's reagent.

2.5 Preparation of TCS Nanoparticles
Similar to N, O-CMC NPs, TCS NPs were prepared by ionic gelation with TPP. The nanoparticles were characterized for size, surface morphology, and zeta potential using DLS, SEM, and AFM.

2.6 Drug Loading and Preparation of 5-FU-N, O-CMC and CRC-N, O-CMC Nanoparticles
The anticancer drugs 5-FU and curcumin (CRC) were loaded into the N, O-CMC nanoparticle matrix through electrostatic interactions with the protonated amino groups of the carrier. The amount of drug loading was optimized, and the drug entrapment efficiency was determined using UV-Vis spectroscopy.

2.7 In Vitro Cytotoxicity and Hemocompatibility Studies
The cytotoxicity of the prepared nanoparticles was assessed using the MTT assay, with HT-29 (colorectal cancer cells) and IEC-6 (normal intestinal epithelial cells). The hemocompatibility of the nanoparticles was evaluated using hemolysis and clotting assays to assess the potential toxicity to red blood cells and the coagulation system.

2.8 In Vitro Drug Release Studies
The release profiles of 5-FU and CRC from N, O-CMC and TCS nanoparticles were studied in simulated gastric (pH 1.2) and intestinal (pH 7.4) environments. The release kinetics were evaluated by measuring the amount of drug released at predetermined time intervals.

2.9 In Vitro Combinatorial Anticancer Evaluation
The combinatorial anticancer effect of the drug-loaded nanoparticles was assessed by MTT, live/dead assay, mitochondrial membrane potential (JC-1), and cell cycle analysis. The efficacy of the combination therapy (5-FU + CRC) was compared with the individual treatments using CRC, 5-FU, and the respective drug-loaded nanoparticles.

2.10 In Vivo Pharmacokinetics and Biodistribution
The pharmacokinetics and biodistribution of the prepared nanoparticles were assessed in Swiss Albino mice following intravenous injection. Plasma drug concentrations were measured using High-Performance Liquid Chromatography (HPLC), and the biodistribution of the drugs was determined by analyzing different organs (liver, kidney, spleen, etc.) at various time points post-injection.

2.11 Histopathological Studies
Histopathological analysis was performed on the tissues from the treated mice to evaluate any morphological changes or organ toxicity following the administration of the nanoparticles. Hematoxylin and eosin (H&E) staining was used for tissue sectioning and visualization under a light microscope.

2.12 Statistical Analysis
Data were expressed as mean ± standard deviation (SD). Statistical analysis was performed using ANOVA or Student's t-test, with p-values < 0.05 considered statistically significant.

RESULTS AND DISCUSSION
3.1 Preparation and characterization of N, O-CMC
In order to produce N, O-CMC, the Chitosan was reacted in alkaline medium, with the carboxylating agent (chloroacetic acid). It is stated that the caroxylmethylation takes place in the following way. In steps 1 of the reaction, the -CH 2 -OH of chitosan is reacted with NaOH which adds the alkoxy group(sodium methoxide) and the group reacts with the one of chloroacetic acid causes O-carboxymethyl substitution. The second step (at 600 C 3 hours) this reaction involves reaction of the -NH 2 groups of the chitosan with the products of the molecules of chloroacetic acid to give rise to the N-carboxymethyl groups and the HCl molecule is lost. The maintenance of the alkaline PH and temperature (60C), are the critical parameters in the experiment. The formulation of N, O-CMC was as follows based on the analysis of FT-IR spectral analysis and the results that are provided in Fig .3.1. The absorption at the spectrums of chitosan averagely yielded 3410 (non), 2924 (UN), 1623, 1513, (delta) (N) 1088, 651/1380, (delta) C/O/C), 651, (because of amino groups), 1153 and 895 cm -1 -H of the cyclic pyranosyl rings. It was found that the most typical peaks in the spectrum of N, O-CMC were located in the 3458 bond stretch along the spectra of -OH, -N-H along the spectra and 1604cm - 1 along with the carboxyl groups spectra. The replacement of chitosan at the carboxyl face location was ascertained at the spectral peak at 1604cm -1 at the FT-IR. Besides this, the prepared N, O-CMC was also concluded to be soluble in water. With the help of this the solubility of the chemically modified N, O-CMC in water was demonstrated. The percentage of carboxymethyl substitution of N, O-CMC was put under the titrametric procedure and was found to be 57 8.

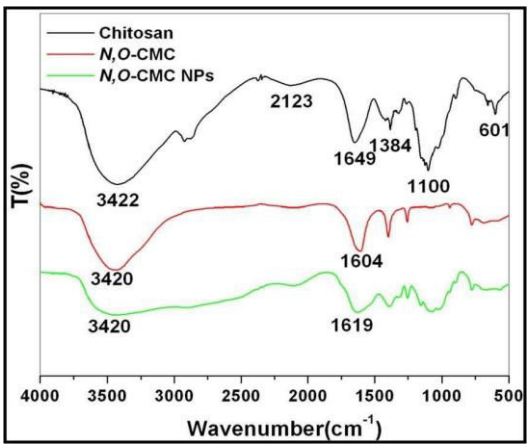

Figure 3.1. FT-IR spectrophotmetic core of chitosan, N, O-CMC and N, O-CMC nanoparticles Spectrophotograph.

3.2 Preparation and characterization of N, O-CMC NPs

The N, O-CMC nanoparticles were obtained through the ionic cross-linking effect, of the TPP phosphate group with the protonated amino group of the N, O-CMC. The FT-IR, DLS and SEM, and the AFM were used to determine the developed N,O-CMC NPs. The final results of the FT-IR spectral analysis of the N, O-CMC NPs was presented in Fig.3.1 and the findings were the findings that revealed the presence of a uniform shift of 1604cm-1 that signified the peak concentration of cross linking N, O-CMC of the Phosphate group of TPP and protonation of the amine group on the N, O-CMC. Also next to it, it is possible to mention the emergence of the peak broadening, which also, appeared in 3420 cm-1 and resulted in the emergence of the TPP-cross-linked N, O-CMC nanoparticles. The size of the particle and the result of the experiment were determined by the use of DSM and AFM analysis, which has been illustrated in Fig.3.2. Fig. 3. Figures 2 (A), (B) and (C), are the result of N, O-CMC NPs characterization size, under condition of DLS, SEM and AFM respectively. This was experimentally determined to be 80mm 30mm which was spherical. In addition, the evidence of the zeta potentials has indicated the value of the N, O-CMC NPs as the value of +46.74 +10 mV has indicated the stability of the particles. The value of the zeta potential was found good and positive implying that it was the N, O-CMC NPs surface created.

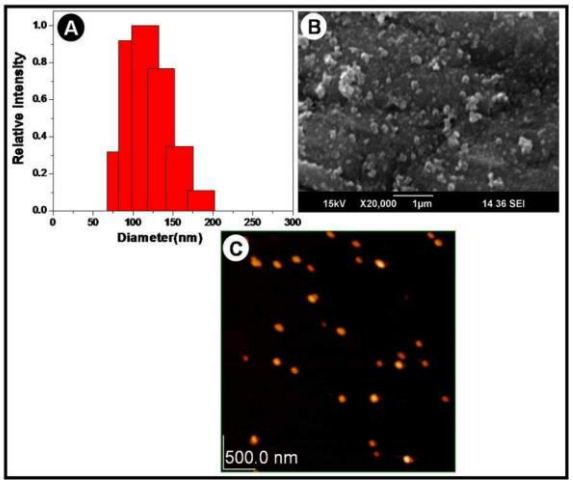

Figure 3.2. Characterization of size of N, O-CMC NPs under (A) DLS, (B) SEM and (C) AFM.

3.3 Preparation and characterization of TCS

Characterization and preparation TCS Preparation and characterization TCS. Preparation and characterization of TCS are being done using the capabilities available in them. Preparation of TCS TCS TCS was prepared by use of TGA where the combination of thiolating reagent and its properties were assessed using the assistance of the FT-IR. During the process of the preparation of the TCS, the -NH 2 functional groups on chitosan became concentrated on an interaction with the carboxylic groups on TGA and formed an amide bond which in turn will be subsequently evidenced by the FT-IR as demonstrated in Fig. 3.3 A that is additive of the FT-IR of chitosan and TCS. Other records obtained in the FT-IR spectral feature include those at 3410 (nu O -H and nu N -H) 2924 (nu C -H), 1623, 1513 (delta N -H), 1088 (nu C -N) 651(delta NH2); delta NH2 record was not observed in TCS, and more importantly, during the reaction, the carboxyl group of TGA is reacting with the amino group of chitosan, and amide is formed.

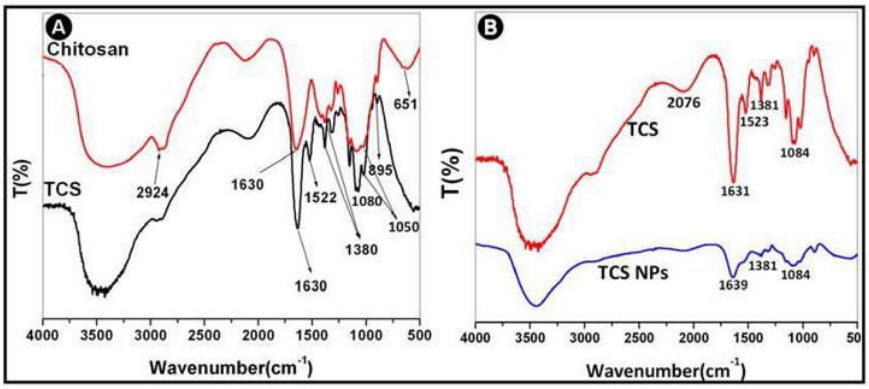

Figure 3. 3. B and A is the FT-IR of chitosan sample, TCS, and TCS nanoparticles.

3.4 Preparation and characterization of TCS NPs

The TCS NPs have been acquired due to ionic cross-linking of the TCS amine functional groups which are stated to be protonated with the negatively functional groups of TPP i.e. the phosphate functional groups (283, 359). The stirring rate of the reagents and concentration of the reagents permits control of the level of cross linking and hence the size of the particles. This FT-IR spectra of TCS and TCS-NPs have been obtained and the result might be summarized as follows: 3410 (nuO -H and nuN -H), 2924 (nuC -H), 1623, 1513 (deltaN -H),1088- nuC N -delta, 651(deltaNH2 -delta) and 895(epimeric -deltaC N -ancia GHEO). 1 This was quite rational given the fact that, the ion A. The average dimension of the TCS-NPs was presumed to be 75nm. The role played by both SEM and AFM resulted in the conclusion as well that prepared TCS NPs in their size was just right. Fig. 3. In 4 B and C, the outcomes of AFM and SEM of TCS NPs are provided. The AFM and SEM provided nanoparticles that had the size of 90 +10nm and 100 +10nm respectively. This also justified the morphology of the formed TCS NPs by the More the SEM and AFM images that verified that the morphology was a sphere. On the measure of Zeta potential, the determination of the degree of charge of surface stability of the prepared NPs systems was carried out. TCS-NPs system determined value of zeta potential was +43.69 mV. The results served to support the intended stability of the established TCS NPs and optimism charge on the visage of the developed TCS NPs. This positive net surface charge could be attributed to the fact that, the number of the protonated amino groups on the surface of TCS NPs are more in number [19].

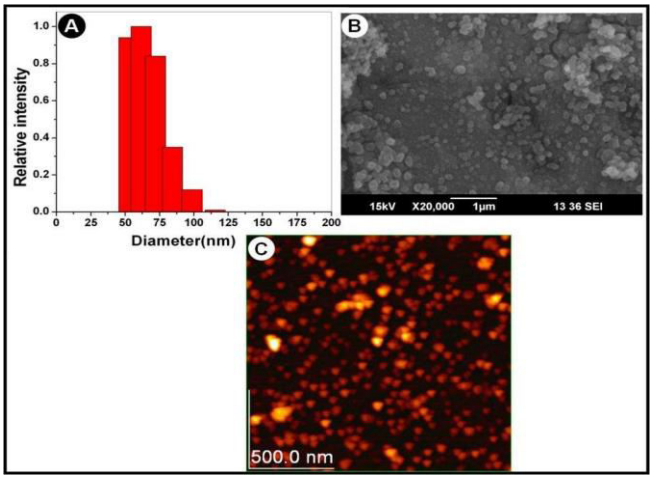

Figure 3. 4. Tabulates the data of size characterization of TCS NPs (A) DLS (B) SEM (C) AFM data.

3.5 In vitro cytocompatibilty of N, O-CMC NPs and TCS NPs by MTT assay

The N, O-CMC NPs NPs and the TCS-NPs MTT were used to establish the in vitro cytocompatibility of the NPs. It was tested with different concentrations of 0.1 to 5 mg/ml of concentration of NPs absence is the positive control (PC) and absence of triton-X (1percent) is the negative control (NC). The outcomes of the experiment of the cells HT 29 and IEC 6 using the 48 hrs incubation period are below: Fig.3.5 A and B. Continuing with the plot, no considerable percentage cell viability of the varying concentrations of the NPs samples under analysis was found against untreated cells. The figure also shows that the percentage viability of the nearly 98 percent of the cells is close to control negative that indicates that all types of concentrations of N, O-CMC NPs and TCS NPs are effective. The findings above demonstrated that the ready TCS NPs are not as toxic to the colon cancer cells (HT29) and the normal cells (IEC 6), and this is a pre-requisite of using a material in practicing medication related. In so doing, the cytocompatibility of the N, O-CMC NPs and the TCS NPs developed were established.

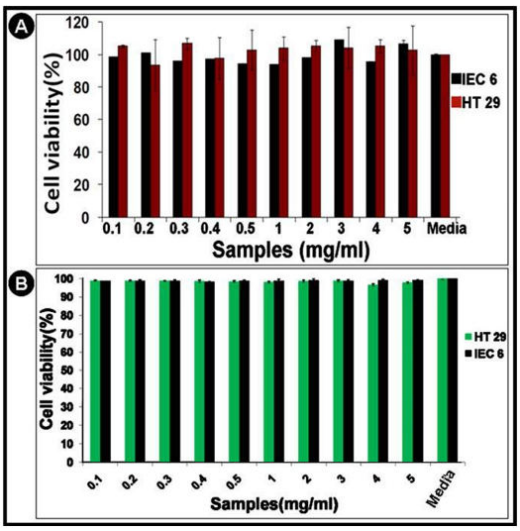

Figure 3. 5. One of the findings of the cytocompatibility study of N, O cytocompatibility NP and TCS NP on the one hand, based on the MTT assay, in the cell line of HT 29 and IEC6 (48hours).

3.6 In vitro hemocompatibility assessment of N, O-CMC NPs and TCS NPs using hemolysis and coagulation assays

The presence of the hemolysis and coagulation tests was used to determine the compatibility of the blood between N, O-CMC NPs and TCS NPs which are presented in Fig. 3.6 and Fig.3.7. Figure (A) and figure (B) represent the graph of hemolysis and coagulation assay respectively. Following one, based on Fig. 3.6A and Fig. 3.7 A, the proportion of hemolysis of the whole sample of the treated blood amounts to less than 5% (379). Fig. 3.6 below (Part B) shows the graphs of the assay clotting of the various concentrations on the PT and aPTT values [20]. The concentration of the values of PT and aPTT of all the samples was normal and can be compared to negative control saline (the normal range of PT: 12-15 seconds and the normal range of aPTT: 25-35 seconds). Therefore, the hemolysis and clotting test demonstrated the hemocompatibility of developed drug carrier regimes.

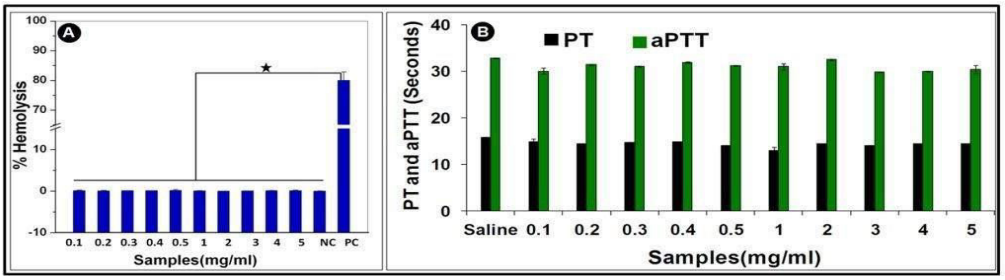

Figure 3. 6. The results Minidisplays N, O -CMC NPs hemocompatibility of N, O -CMC NPs under hemolysis (A) and coagulation (B) test.

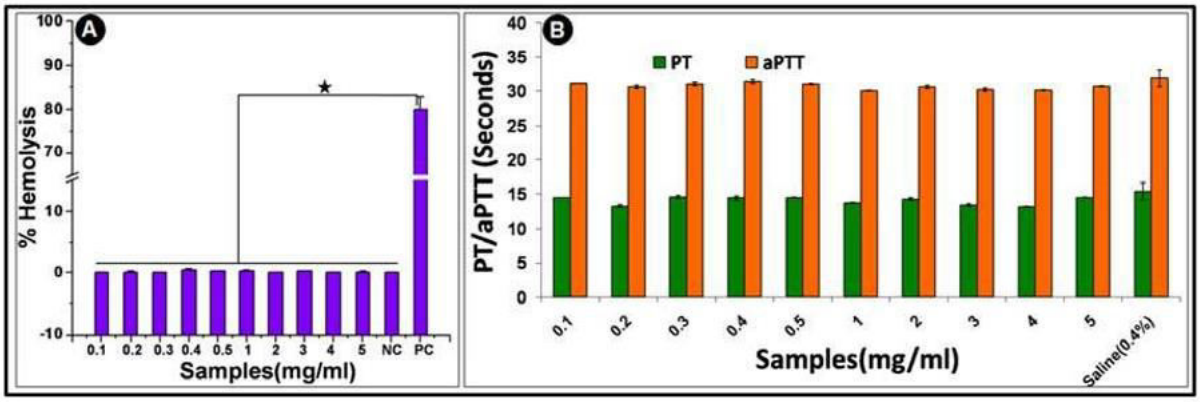

Figure 3. 7. Demonstrates hemocompatibility of TCS NP based on hemolysis (A) and coagulation (B) tests.

3.7 Synthesis and characterization of 5-FU-N, O-CMC NPs and CRC-N, O-CMC NPs

TPP-linked CRC-N, O-CMC NPs, 5-FU-N O- CMC NPs. The BSA had been inculcated to the nanoparticles since this helped to stabilize the BSA. The real systems of nanoparticles were varied to the concentration of 22.5mg of N, OCMC and 5- FU of 5 and 10 mg, respectively. Crystallization of the CRC is provoked by the rise of the concentration of the drugs and entrapment of 5-FU were not enhanced. The optimized systems were further characterized, in-vitro combinatoric analyses of anticancer and in vivo biodistribution and pharmacokinetics analyses were done [21].

Fig. 3.8 shows the findings regarding the size distribution of nanoformulations of 5- FU and CRC, achieved during the impact of applying the DLS and SEM. The size of 150 + 20 + 100 + 20 of the 5-FU-N, O-CMC NP and the CRC-N, O-CMC NP was validated by the information respectively. It was also observed during results of the SEM that the manufactured nanoformulations underwent transformation to the spherical nature. It was established that the zeta potential of the CRC-N, O-CMC NPs, and 5-FU -N, O-CMC NPs were +23. 4 +5.08 mV and +38.7 +6.32 mV respectively (Table 3.1). The nano-particles and the positive charges were in good stability as indicated by the values of zeta potential. The discussion of the difference between the values of zeta potential of the CRC-N, O- CMC NPs and that of 5-FU-N, O- CMC NPs, is discussed below. This may be attributed to the fact that positive zeta potential of the CRC-N, O-CMC NPs and 5-FU-N O- CMC NPs is a result of remaining protonated amino groups of the NPs. The findings of the entrapment of the 5FU/CRC in N, O-CMC NPs can be explained by the following: the unprotonated amino groups of N, O-CMC are also present as major functionality of the CRC and 5-FU. This way, loading / entrapment of the CRC with the N,O-CMC NPs array will happen just as in the loading/ entrapment of the CRC with the N,O-CMC NPs matrix in the case of the CRC-N,O-CMC NPs, by the electrostatic interaction of the protonated amino groups of the N, O-CMC NPs NPs with the carbonyl (2 carbonyl functionality per one CRC) groups of the CRC and the hydroxyl groups(2 hydroxyl functionality per one CRC). Alternatively, in the 5-FU-N, O-CMC NPs, chemistry of interaction between the FU and the HN, of the O-CMC nanoparticle. The availability of 2 carbonyls and 1 fluorine of 5-FU and protonized amine of the N, O-CMC NPs are the significant functionalities. Surface charge and therefore, zeta potential of the resultant CRC-N, O-CMC NPs/5-FU-N, O-CMC NPs depends upon the strength of the electrostatic interaction of the drugs to the carrier nanoparticles (CRC/5FU and carriers N, O-CMC as seconded by the nature of the surface interaction). Just like in the previous example, the electronegative functionalities of drug; CRC are more increased when compared to the electronegative functionalities of drug 5-FU (in the second case). The positiveness of N, O-CMC NPs is lesser in the former i.e. CRC-N, O-CMC NPs the latter i.e. 5-FU-N, O-CMC NPs as compared to the former case. At the present stage zeta potential of the two systems is already in the range of stable values and this is why, it is colloidalally stable [22].

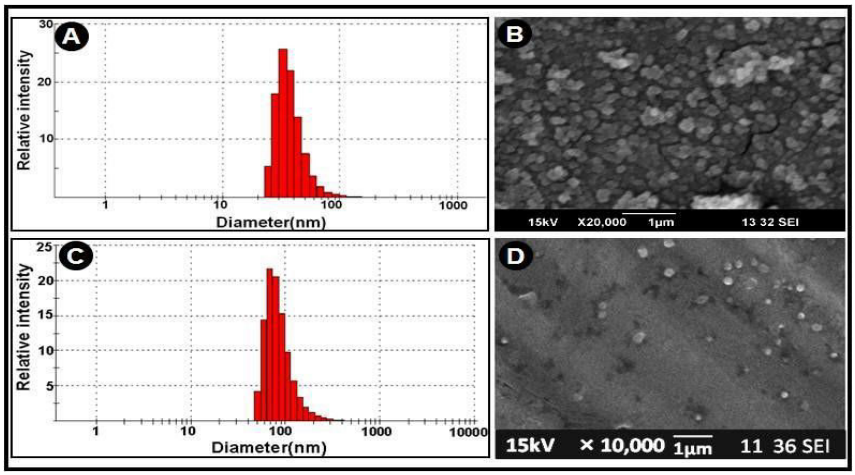

Figure 3. 8. The size characterisation (DS) data of 5 -FU-N, O-CMC NPs and the O-CMC NPs using DLS and SEM where (A) and (B) 5-FU-N, O-CMC NPs, (C) and (D) CRC- N, O-CMC NPs.

Systems	Zeta potential (mV)	Entrapment efficiency(%)	Loading efficiency(%)
5-FU-*N,O*-CMC NPs	+38.7 ± 6.32	47.96 ± 2.3	33.78 ± 7.59
CRC-*N,O*-CMC NPs	+23. 4 ± 5.08	84.26 ± 1.46	50.63 ± 3.83

Table 3.1. Displays the values of zeta potential, entrapment and loading efficiency of 5FU-N, O-CMC NPs and CRC-N, O-CMC NPs.

3.8 Characterization of 5-FU-N, O-CMC NPs and CRC-N, O-CMC NPs by FTIR spectra

The FT-IR spectral analysis of 5-FU- N, O- CMC NP i.e., a, b, c, d e n, e yielded the following results as depicted in fig. 3. 9. The maximums of the FTIR spectrums of N, O-CMC nanoparticles were received at 1630 by - N -H vibrations of the carboxyl-methylated -N -H group, 1068 by the secondary hydroxyl group (characteristic spectrum of cyclic alcohols -C -O stretching), and the pyranosyl ring of 895 cm respectively. Available were the FT-IR spectrals maxima of CRC of archetypal form 3510 (bending vibrations of phenolic -OH), sharp absorption at 1605 (benzene ring stretching vibration), T -C =O and C -C vibrations at 1502 and the olefinic -C -H bending vibration respectively. N, O -CMC NPs shifted in the entrapment of CRC in CRCN, OCMC NPs. There were common FT-IR spectra of the 5-FU that included peaks of 3000 -2900 cm the -C-H reactions, and FT-IR frequency of 1425- -C-N and -C rings as well as 1344 cm -1 which was the pyrimidine resonance. The -C-O and -C-N vibrations were

observed as 1180, 1639 and 1243 cm -1 (88, 102,386) as well. The 5-FU-N, O-CMC NPs which are entrap in 5-FU correspond to the adjustment and enhancement of the peak strength in 1630 cm-1 since the carbonyls and the fluorine group of 5-FU bind the intermolecular hydrogen bond with the produced CRC-N, O-CMC NPs (382).

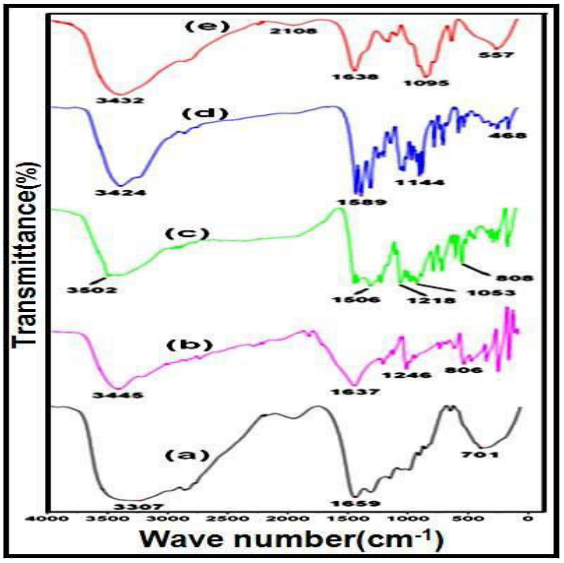

Figure 3. 9. Plot the FT-IR spectrophotometers of the obtained spectral analysis findings; (a) BSA, (b) 5-FU, (c) CRC, (d) CRC-N,O-CMC NPs and (e) 5-FU-N,O-CMC NPs.

As a result, CRC-N, O-CMC NPs, and 5-FU-N were turned into high stability O-CMC NPs on cross-linkion of the ions of 100 20 nm, 150 20 nm and 5-FU-N (234). The interdependence of the N, O-CMC NPs and the drug entrapment is enabled because of the use of the hydrogen bonding alongside the electrostatic bonding. These sizeable functionalities were carboxymethyl group as well as hydroxyl group of N, O-CMC with carboxyl, hydroxyl and methoxyl group of CRC (via the example of CRC-N, O-CMC NPs) and carbonyl and fluorine group of 5-FU (via the example of 5-FU-N, O-CMC NPs). The chemical interaction of the entrapment of the drug was affirmed with the help of FT-IR spectrometer.

3. 9. The efficiency of the enterprise (EE), loading efficiency (LE) and in vitro drug release profile of 5-FU-N, O-CMC NPs NPs and CRC-N, O- CMC NPs.

EE and LE of 5-FU and CRC optimum nanoformulation were 47.96 2.34 and 33.78 7.59 5-FU and CRC respectively. Its EE and LE of CRC -N, O-CMC NP were superior over 5-FU- N, OCMC NP and this can be attributed to the reason that 5-FU is a hydrophilic substance. The biological explanation is that, CRC being a hydrophobic drug and therefore, owing of CRC with N, O-CMC is more efficient than loading it with a hydrophilic drug; 5-FU. Fig. 3.10 is the release of the nanoformulations of 5-FU /CRC in vitro at pH seven point four and in pH four point five. A and B denote the profile of 5-FU- N O-CMC NPs and CRC-N O-CMC NPs release.

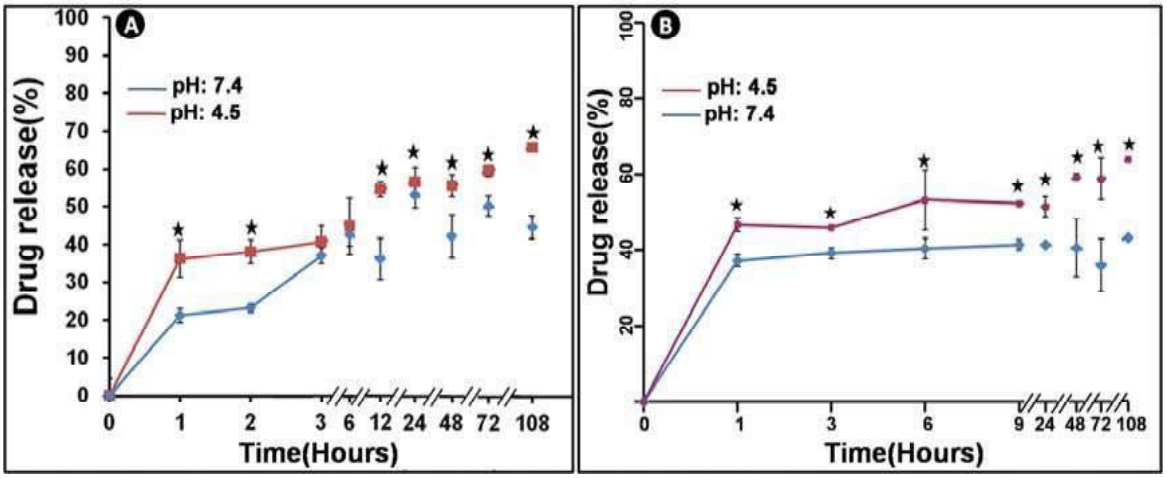

Figure 3. 10. The non-linearity between the scales (p of less than 0.05, statistical significance) is indicated by release profile of (A) 5-FU-N, O 8 CMC NPs and (B) CRC-N, O 8 CMC NPs in in vitro conditions that are pH 7.4 on X-axis.

It was established that 5-FU-N, O -CMC NPs release profile at pH 7.4 was 20-25 percent at 1hour burst release, progressive and progressive release 5-FU at 20-25 percent at 1 hour and 108 th hour. It has a higher release in acidic pH with 40 per cent released in the first 6 hours and the long term release of 60-65 per cent at time 108 th hour. The results of the initial burst release profile of the CRC by the CRC-N, O-CMC NPs of 37.19 + 1.3 percent are attributed by the presence of the drug stuck around the surface

of the drug. The more the release, the more it would be to 43.15 +/-7.0 percent to 108 th hour. Following 1 st hour, release pattern value was 46.55 + 1.58 percent at acidic PH. Upon conversion of time (1 st to 108 th hour) the shift in the discharge of CRC will lead to an upward shift in 63.64 + 5.51% of the drug. The mechanism of releasing drugs during in vitro practicing can be attained in the following steps involving initial release burst caused by the drug that is adsorbed on the surface, low and gradual release caused by diffusion and slow decay of N, O-CMC NPs. To degrade N, O- CMC NPs, the hydrolysis reaction was performed and it involved breaking down of glucosamineglucosamine linkage, glucosamine- N-acetyl glucosamine linkage, and N-acetyl glucosamine- N-acetyl glucosamine linkage. This is due to release in acid pH being enhanced since N, O-CMC NPs are sweltering and as a result of the presence of a protonated N, O-CMC amino group which is then degraded. This is advised by the fact that the 5- FU/CRC in N, O-CMC NPs nanoformulations were more liberated in acid PH. This is desirable compared to the reduction on the non selective introduction of the free drug in the circulatory blood and subsequent organ poisoning. Moreover, the nanoformulations can also be selective of the release of the drugs to the acid pH such as endocytic vesicles (endosome and lysosome) and tumor tissues.

3.10 In vitro combinatorial anticancer evaluation

It was also established in vitro with the result of the percentage cell death measurements using mitochondrial membrane potential(JC-1) and cell cycle analysis results that N, OCMC nanoformulations of 5-FU and TCS nanoformulations of 5-FU had the desired anticancer property. The outcome of both these experiments was as follows.

3.10.1 MTT and live dead assay

The first point that was established was that the combinatorial anticancer effect of bare and drug loaded N, OCMC NPs / drug loaded TCS NPs boiled down to the confirmation of the MTT assay at varying concentration of varying incubation time; 24, 48 and 72 hours. The data provided on Fig 3.11 indicates the measurements of the time of MTT procedure of the drugs CRC, the 5-FU, the mixture of the bare drugs, CRC-N, O-CMC NPs, 5-FU-N and O-CMC NPs and the combination of the drugs at 20 4mio/l invigiation of the incubation time of 24, 48 and 72 hrs. The cell death was best achieved with the combinatorial treatment as the result was 86 with cell death percentage of 90, 95, and 46-50 in the cell sample, 24,48, and 72 hours incubation of the specimens.

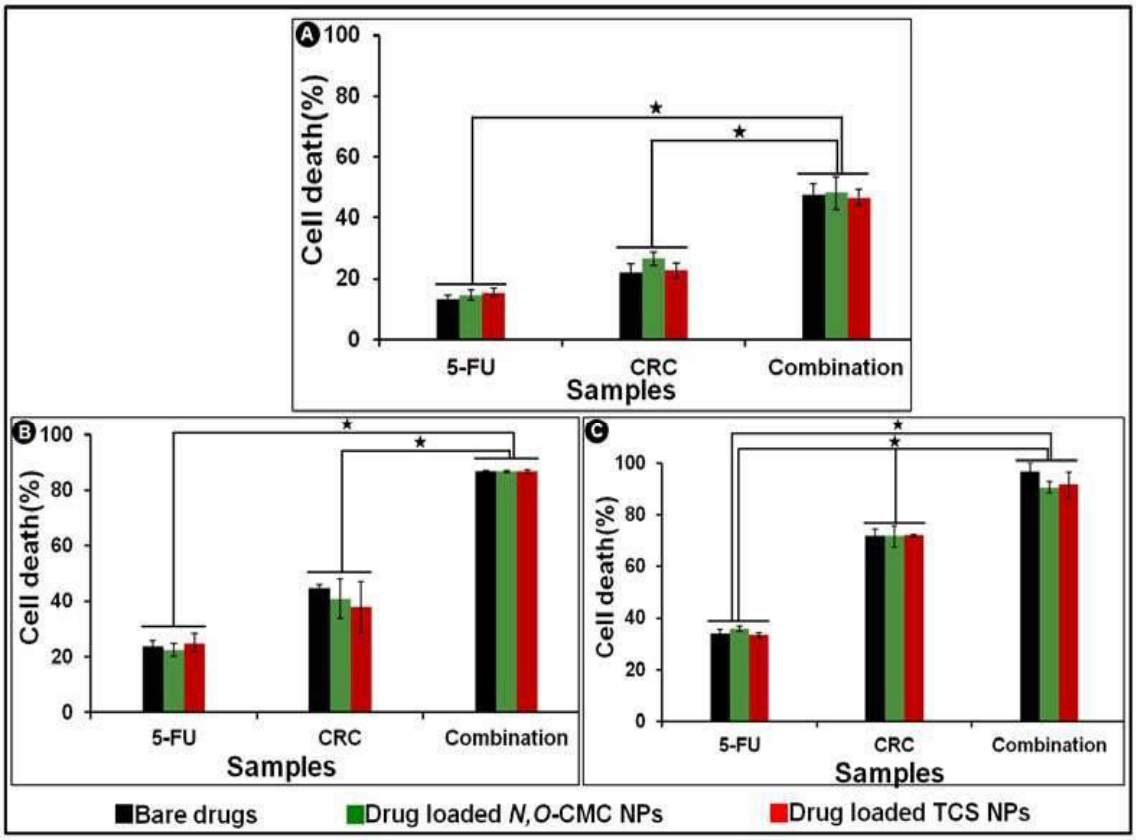

Figure 3. 11. A, B, C represent cell death assay of the cell under the treatment of CRC, 5 -fU, combination of bare drugs and CRC- N, O-CMC NPs and 5 -fU- N, O- CMC NPs and combination of NPs respectively after 24, 48 and 72 hours respectively with the assistance of MTT to the cell assay.

The values of CI have been realized. It was ascertained that the percentage value of cell death of the sample treated cells (after 48 hours) were estimated as 22.49 +2.36, 40.85 + 7.05, 86.72 +0.44, 24.96 +2.36, 37.79 + -6.49 and 86.72 +0.44 respectively in 5-FU-N, O-CMC NPs/CRC-N, O-CMC Cell death The values were also less than one in both the tests (0.86 ± 0.088, 0.85 ± 0.088 and 0.84 ± 0.085 respectively when combined with bare drugs, drug loaded N,O-CMC NPs system, and drug loaded TCS NPs system respectively) compared to Table 3.3. In this respect, CRC /CRC-NPs supplement the anticancer activity of the 5-FU/5-FU-NPs at the level of 2019hours in the HT 29 cells.

System	Bare drugs	Drug loaded *N,O*-CMC NPs	Drug loaded TCS NPs
Combination Index(CI)	0.86 ± 0.088 (<1)	0.85 ± 0.088 (<1)	0.84 ± 0.085 (<1)
Concentration of 5-FU(μM)	20	20	20
Concentration of CRC(μM)	20	20	20

Table 3.2. The index of the samples (CRC/5 FU, CRC-N, O CMC NPs/5 FU-N, O CMC NPs and CRC-TCS NPs/5 FU-TCS NP) of the samples with the use of the 48 hours HT 29 cells.

Thus, it was planned to conduct additional confirmogenic tests (live dead, mitochondrial membrane potential and the cell-cycle-analyses measurements) at 48hours of the concentrations 20 00 CREC/CRC-NPs and 20 00 5-FU/5-FUNPs. Fig.3.12(A to J) contains result obtained in the analysis of the live dead assay (vast majority of the cells were alive), and cell data which depicted cell death of the cell of either bare or drug loaded nanoparticles combined treatment compared to the undruged cell. The red birefringence of the cells was indicated to be higher in the mixture of drugs / drug loaded NPs (as in D, G and J). Compared to the individual drugs or drug loaded nanoparticles at 48hours, treatment combustion had a higher cell death.

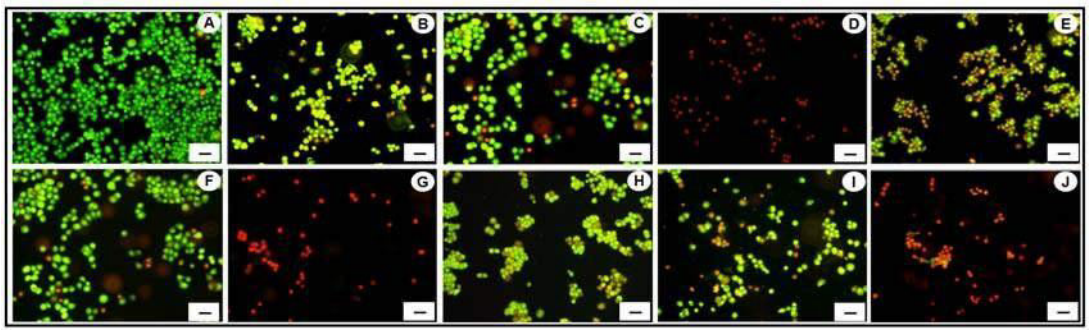

Figure 3. 12. They include analysis of cell death of the cells in the live dead assay (48hours) that had been controlled or treated with 5-FU or O-CMC NPs (all experiments involving three, n=3 and triplicates).

3.10.2 Mitochondrial membrane potential measurements

Observed alterations in the values of the mitochondrial membrane potential in response to the treatment of the sample (in the HT 29 cells during the experiment period of 48 hours) and the observed variations in the value was indicated in Fig.3.13 and Fig.3.14 respectively in the form of flow cytometry. In Figure P2 and P3 below in which A is the flow cytometric dot plots, and C is where the red cytometric is the green cytometric fluorescent respectively and proportional percent number of the cells with good-health-condition of mitochondria and the set of that which were in the apoptosis states or are dead respectively. Fig. B is the plots of the percentage of cells to have green fluorescent (percentage of apoptotic /dead cells) against different samples. Fig. B (that is, the percentage of cells which are represented by the percentage of fluorescing or the number of cells that have apoptotic or dead mitochondria) was determined as 5 + 2.96, 31.75 + 3.32, 18.3 + 4.1, 72.6 + 6.50, 29 + 1.84 and 75.15 + 5.97 percent of the control, CRC, 5-FU and a combination of 5-F respectively.

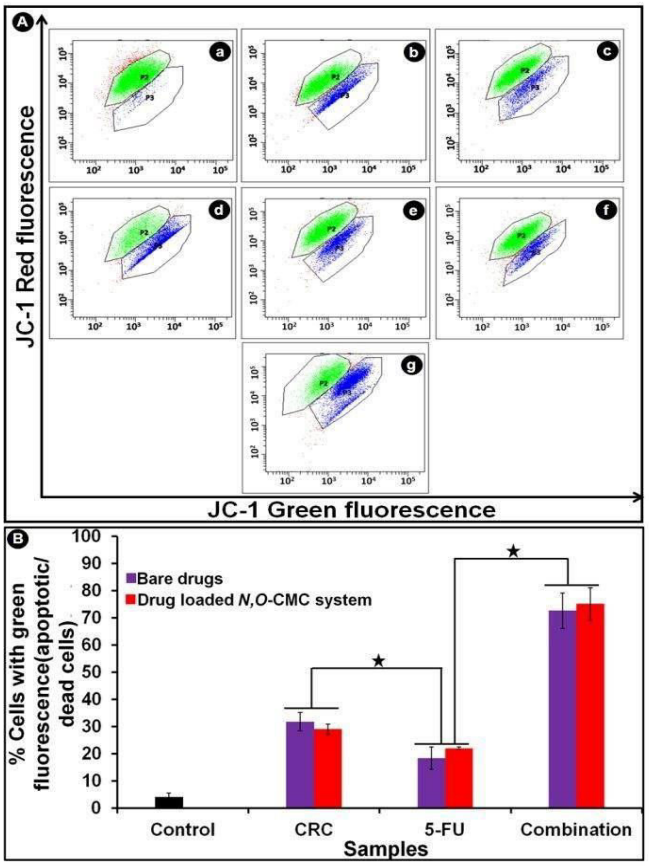

Figure 3.13. A flow cytmetric measurement of the combinatorics of the anticancer action of the CRC-N,O-CMC NP, 5-FU-N,O-CMC NP, and a combination of the basidium, of the controls, the treatments, and their combination of the percent apoptotic/dead cell under treatment, respectively, of the controlled HT 29 cells are as follows:

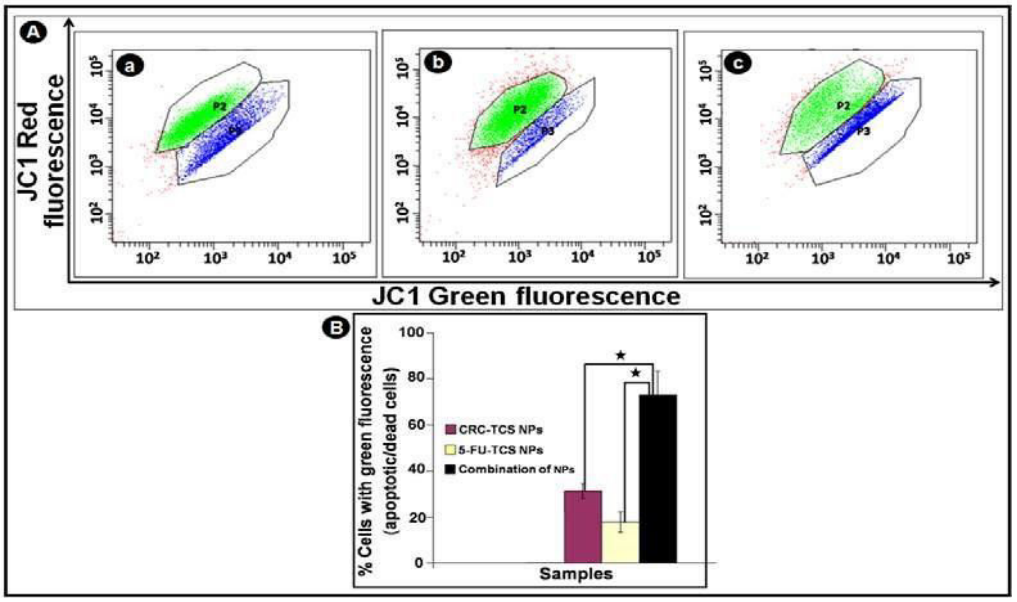

Figure 3. 14. The cytotoxic activities of CRC-TCS NP and 5-FU-TCS NP against the cells were compared using the quantitative part of the graphical data via the percentage, dead cytosatisfied/apoptotic cell (green fluorescence) where f, g and h represent the cell count that was subjected to the fungus exposed to CRC TCS NP, 5-FU-TCS NP after the 48 hours of treatment was applied (A), (B) was used.

It was therefore the mitochondrial membrane potential that supported ITT and live dead. It was equally suggested that combinatorial drug/drug loaded NPs system presents a much greater anticancer activity compared to the individual i.e. bare and drug loaded system. Past research had already made the claim that the lack of the mitochondrial membrane potential resulted in cascaded apoptosis caused by CRC. It would also enable our study to investigate the change of mitochondrial membrane potential (e.g. the outcome of the HT29 cells being exposed to the treatment of the CRC/CRC-N, O-CMC NPs/CRC-TCS NPs would lead

to the shift). Consequently the percentage of the most appropriate proportion of apoptosis was determined to be 29-30 percent of the apoptotic cells in treating CRC/CRC-N, O-CMC NPs/CRC-TCS NPs. The low percentage of the apoptosed cells (15-17%), could be observed in the case of the apoptosed cells of 5-FU/5-FU-N, O-CMC NPs/5-FU-TCS NPs-treated cells. It can be the result of the alteration of the mitochondrial potential that occurred as a result of apoptosis of 5FU induction (402). The percentage of apoptotic cells are shown to be amplified by an astronomical value in lieu of the combinatorial treatment, CMC/5-FU, CRC-N, O-CMC/5FU-N, O-CMC NPs/5FU-TCS NPs. Its cumulative effects on individual treatment are high, and the effect is higher than the other. The reason is that, CRC are those that can sensitize the induction of apoptoses of HT 29 cells with the use of 5-FU; inhibition of cyclooxygenase-2(COX-2) at both mRNA and protein levels (over expressed in colon cancers). COX-2 down regulation and synergy of CRC and 5-FU on as far as anticancer activity is concerned had been previously known.

3.10.3 Cell cycle analysis

It also became apparent that the anticancer properties of 5-FU/CRC-N, O-CMC NP as Combinatorial anticancer were further confirmed and quantified using the cell cycle analysis and published in Fig.3.15 and Fig.3.16. The following figures where A is flow cytometric histograms of the case with samples as follows, (a) control, (b), (c), (d), (e), (f) (g) and where 5-FU-N,O-CMC NPs/CRC- N,O-CMC NPs. These are the points of the flow cytometeric dot map of G 0/G1 (P3), S (P4), G 2/M (P5) as well as apoptotic (P6). The proportion of cells in both stages was computed and the charts were plotted against the concentration of sample and it is displayed in Fig. 3.16 (B) bare drugs, (C) drugs loaded N, OCMC NPs. The percentage of the cells of apoptotic / dead phase under B and C were found to be 27.65 +1.34, 23 +1.41, 60.8 +1.84, 22.9 +9.19, 26.3 +3.25 percent of the CRC, 5-FU, CRC/ 5-FU, CRC- N, O-CMC NPs, and 5- FUN, O- CMC NPs respectively.

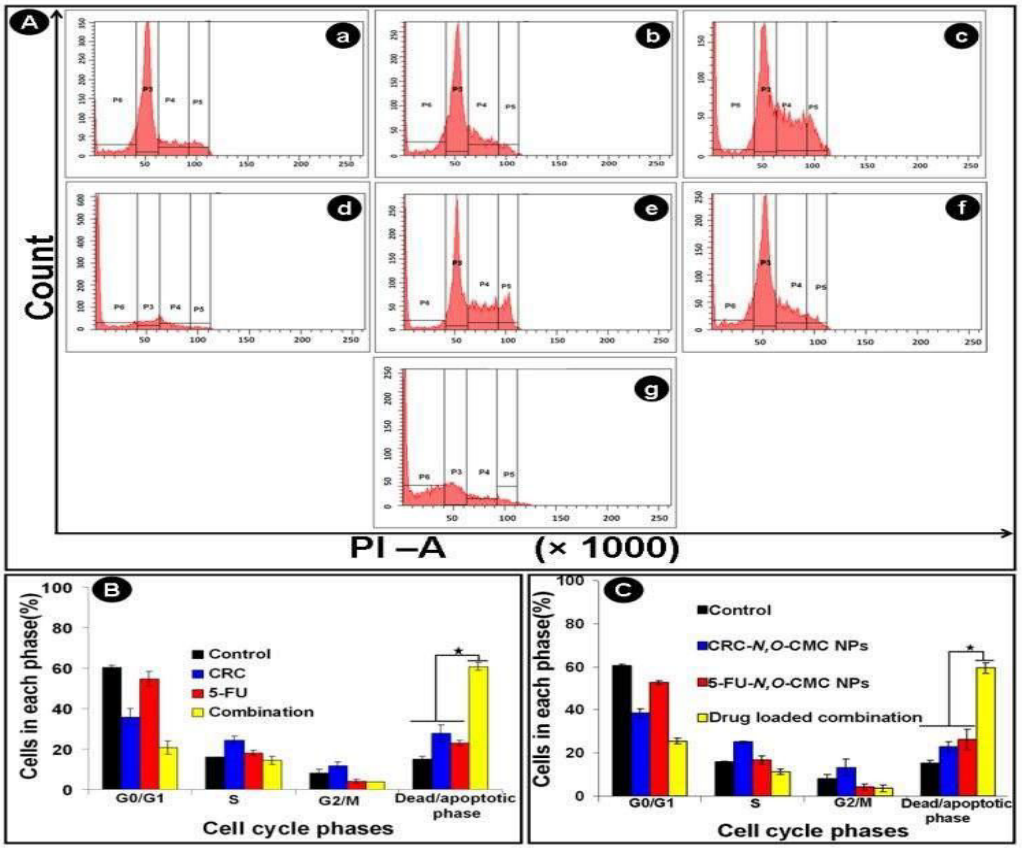

Figure 3. 15. The flow cytometric histograms of the quantification of the combinations of the anticancer effects of the CRC-N, O- CMC NPs on 5-FU, N-O -CMC NPs and the combination of the two on the cells respectively, after cell treatment of the cells was as illustrated below:

Fig. 3.16 shows the results of the cell cycle of the loaded drug of the commodity (HT 29) overall treated cells. Where again, A and B represent the flow cytometric histogram and corresponding graphs of the percentages of the number of the cells in every phase of the cell cycle respectively. Fig. 3.27 B allowed to reveal the percent proportion volume of the cells in the phase apoptotic/dead as 23.8 +/-4.81, 22.95 +/-2.19 and 59.15 +/-2.33[CRCTCS NP, 5-fU-TCS NP and the two NPs respectively].

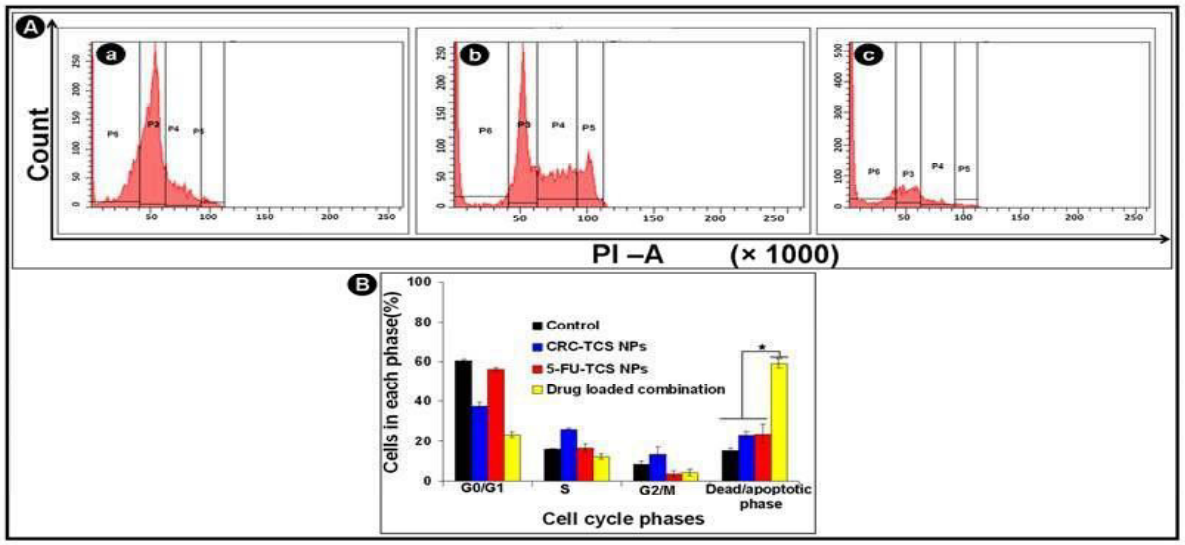

Figure 3. 16. In the calculation of the action of combinatoric of anticancer effect of the CRC-TCS NPs and the 5-FU-TCS NPs with the measurements of the percentages on the phases of the cell cycle after treatments with the CRC-TCS NPs and/or the 5-FU-TCS NPs (combination of CRC-TCS NPs/ 5-FU-TCS NPs), (a) and (b) and (c) were the values of the percentages of the cells at the phases of the cell cycle after treatments with the CRC

CRC and 5-FU are natural inducers of the cell death of colon in apoptotic mode since they inhibit G2/M and S phases respectively. Consequently, the P6 (apoptotic) of cells in the percentage of cell accumulation would be low in cases of cells subjected to individual nanoparticles and bare drugs as well. As a group, however, we can observe an increase in the anticancer response and the resultant, an apoptosis 5-FU/CRC in bloc, 5-FU-N,O-CMC NPs/CRC- N,O-CMC NPs and 5-FU-TCS NPs of 60.8 + 1.84, 59.45 + 0.35 and 59.15 + 2.33 respectively. The outcomes of the cell cycle also supported the fact that there were proliferated anticancer activity of the combinations of the CRC/5-FU, CRC-N, O - CMC NPs/ 5- FU-N-O - CMC NPs, and CRC-TCS NPs/ 5- FU-TCS NPs.

This manner displayed the anticancer effect of the nanoformulations in vitro with the aids of various assays in case of the HT 29 cells. The data of MTT, live dead tests not only supported the upsurge of anticancer characteristics of the combinatorial formulation in comparison with the solitary nanoformulations. On top of that, the cell cycle analysis was employed to support the findings by the application of the mitochondrial membrane potential. Thus, anticancer activity of the nanoformulations that had been found to be combinatoric was competitive to treatment of high percentage of apoptosis/cell death when administered singly. The interplating effect on the COX-2 -catenin inhibition may be the synergistic growth of the anticancer effect that has the possibility to sensitize the colon cancerous cells to 5-FU.

CRC and 5-FU work singly resulting in cell killing of the colon cancer in the following ways that were also equally discussed. The CRC can effect apoptosis of cancer cells of colon by various pathways. Two of them are that the two sets of genes caused p53-mediated apoptosis upon the action of stress signals via the p21/waf1 and GADD45 stress platforms. The functions of these genes in gagging involve the inhibition of the rise in the cell of Bax that induces the apoptotic process of the cell. Fig. 3.17 A. Diagrammatic illustration of p53 mediated cell cycle control of CRC. p53 controls the expression of various proteins which regulate the cell cycle, p21 (Waf 1). It further prevents complexation of cyclin dependent kinase (Cdk)-cyclin and consequently the arrestment of the cell cycle and apoptosis is inhibited due to the insertion of the 5-FU (a pyrimidine analogue) to the DNA and the RNA (Fig.3.17 B). It is dead as well, FdUMP also suppresses the thymidylate synthase (TYMS) and consequently, the formation of pyrimidine thymidine which is required in the synthesis of DNA (404). The engagement of the COX-2 inhibition is the one that is involved in the combination and is what enhances cell death. To this end, the COX-2 mRNA/ protein expression that is induced in the colon cancer cells after initiation of CRC agents blocks replication of the anticancer activity of 5-FU (137, 139). The therapeutic impact of CRC and some of these comparative to 5- FU, was determined as being combinatorial by examining in scale reports in the in vitro and in vivo setting on various cancers and our finding that were highly interrelated with the already existent reports.

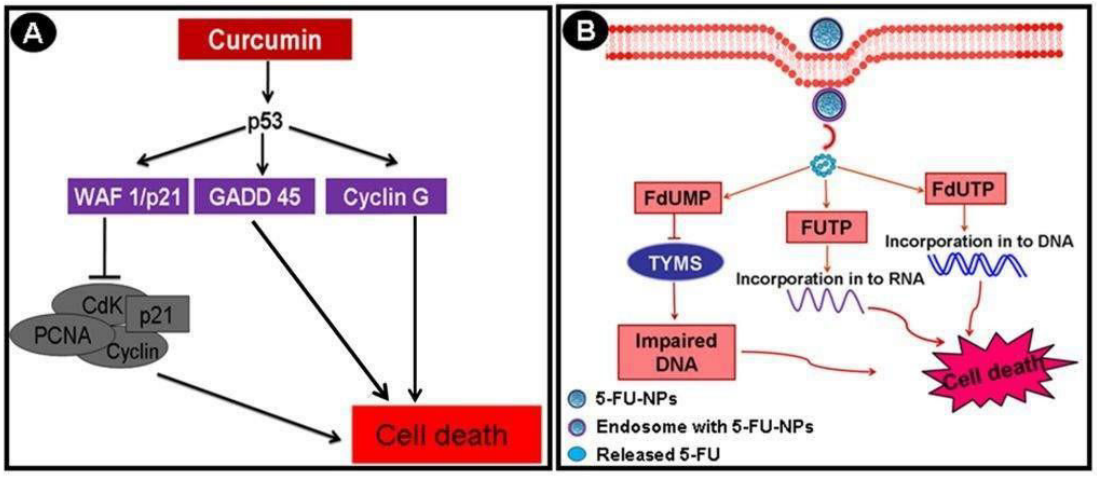

Figure 3. 17. Approach will refer to the route that will be applied in order to imply the anti-cancer effect that is being induced by CRC on HT 29 cells and (B) route that will be used to imply the anti-cancer effect that is induced by 5-FU on HT 29 cells.

3.11 In vivo pharmacokinetics and biodistribution analysis in Swiss Albino mice

Fig 3.18 (A), (B), (C) and (D), depicts the pharmacokinetics and biosixus of the CRC- N, O-CMC NPs and 5-FU-N, O- CMC NPs respectively at the end of the intravenous treatment of the drug respectively at 72 hours intervals in the Swiss Albino mice. The apparent measure was the figures of 5-FU plasma concentration verses time and CRC plasma concentration verses time of Fig. 3.29 A and C in the drugs, which remains the unbelievable contrast between the wicket formulations and the nanoformulations of drugs. At 0.25 hours, the plasma concentration of 5-FU was high 69.16 +0.64 5g/ ml and the further extension of the time resulted in a diminution in the plasma concentration to an insignificant level of the twelfth hour. This fact can be likened with such reported literatures.

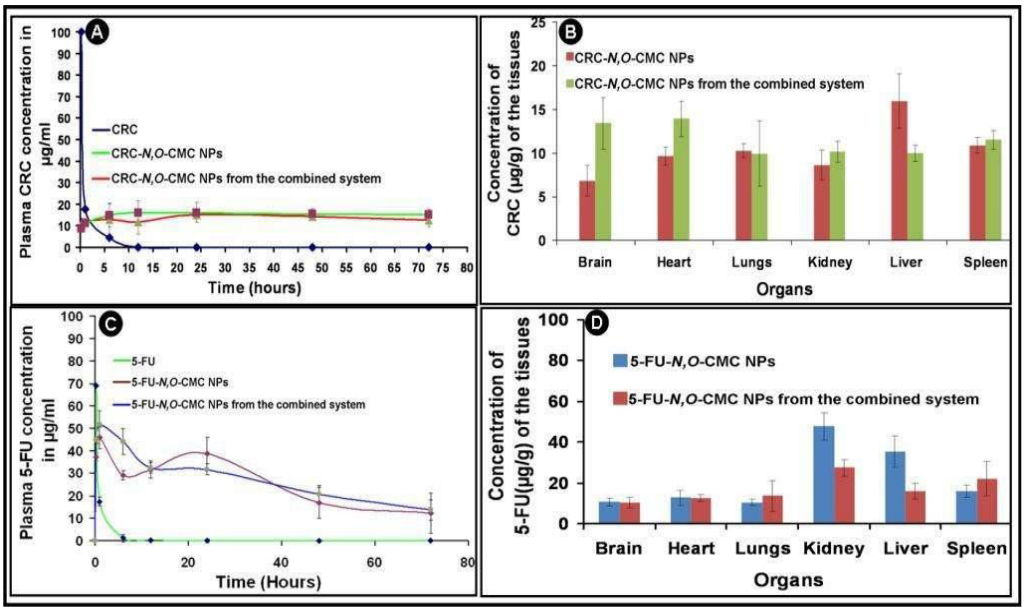

Figure 3. 18. A, B, C, D Yet A, B, C and D represent, respectively, the pharmacokinetics and biodistribution of CRC- N, O-CMC NPs and 5-FU-N, O-CMC NPs of the Swiss Albino mice at the times (A) of 72 hours, (B) of time, (D) the profile of the biodistribution of the two drugs.

Peak plasma level; Cmax 45.98 was achieved in 1 st hour But the parallels with the naked 5-FU (registered Cmax 69.16 -0.64 0.25hours and plasma level of 5-FU was produced by the NPs dropped over time) held plasma concentration of forces 5-FU produced by NPs.

Parameters	Units	Bare 5-FU solution	Bare CRC solution
T_{max}	Hours	0.25	0.25
C_{max}	µg/ml	69.16 ± 0.64	100 ± 5.3
AUC $_{0-t}$	µg/ml*Hour	105.82 ± 2.58	158.13 ± 21.14

Table 3.3. When the Swiss Albino mice were intravenously injected with the naked 5-FU and CRC solution, the end of the pharmacokinetic of the solution was found to be at 72hours (to 72hours) (as shown in Table).

Parameters	Units	5-FU-*N,O*-CMC NPs	5-FU-*N,O*-CMC NPs from the co-administered system
T_{max}	Hours	1	1
C_{max}	µg/ml	45.98 ± 4.86	51.76 ± 6.14
AUC $_{0-t}$	µg/ml*Hour	2595.92 ± 478.91	1943.32 ± 260.96

Table 3.4. These are the pharmacokinetic parameter, which were determined on 5-FU-N, O- CMC NP and 5-FU- N, O-CMC NP of the concomitant system on the Swiss Albino mice (in 72 hours).

The 5-FU-N,O-CMC NP of AUC0-t value and 5-FU-N,O-CMC NP of the co-administered system were 2595.92 =478.91 and 1943.32 =260.96 respectively which are very high in comparison to the co-administered system 5-FU control value of 105.82 =-2.58 5.

Parameters	Units	CRC-*N,O*-CMC NPs	CRC-*N,O*-CMC NPs from the co-administered system
T_{max}	Hours	24	24
C_{max}	µg/ml	16.11 ± 4.58	15.07 ± 0.89
AUC $_{0-t}$	µg/ml*Hour	1105.71 ± 258.42	988.5 ± 172.7

Table 3.5. The calculated pharmacokinetic parameters with the help of the CRC- N, O CMC NP and the CRC- N, O CMC NP of the system that was co-injected only after the intravenous injection in the mice of Swiss Albino (72hours).

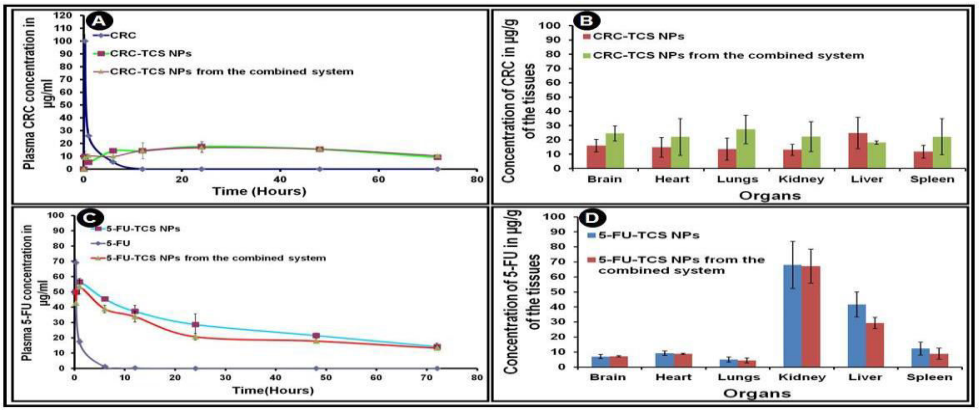

Fig. 3. 19 (A) (B) (C) (D): Data Pharmacokinetics and biodistribution of the CR- TCS NPs and the 5-FU- TCS NPs in the Swiss Albino mice at 72 hrs where (A) and (C) is only the complete pharmacokinetic profile of the CR- TCS NPs and the 5-FU -TCS NPs respectively, and (B) and (D) is the complete profile of the biodistribution of the CR- TCS N

The pharmacokinetic parameters that were derived on the CRC-TCS NPs, 5-FU-TCS NPs, and the behavior of the corresponding co-administered base, (combination of 5-FU-TCS NPs and CRCTCS NPs) and the respective base drug solutions are presented in Table 3.7 and Table 3.8 after intravenous administration. Both the plasma concentration 5-FU and the CRC a time 30A and C are a complementary term in expressing the existence of excellent diversifications in the case of the unprotected and the nanoformulations of the drugs. The occurrence of a high peak plasma concentration; Cmax of 56.51 ± 2.24 and 53.25 ± 6.61ug/ml at 1 st and hour respectively following the administration of the samples was noted in the plasma concentration profile of the 5-FU sample (5-FU-TCS NPs) and the group of drugs (combination of 5- FU- TCS NPs R and the CRC- TCS NPs) respectively when the samples had been administered. Plasma 5-FU system and 5-FU co-administration system exhibited a decline of plasma concentration- time profile with time. The concentration of 5-FU by the NPs in the plasma was thus 5-FU ug/ ml as opposed to the concentration of the unbare 5-FU(maximum concentration of 69.16 difference of 0.64 ug/ml at the time of 0.25 hours and a

fall at the time of 12hours).

Parameters	Units	5-FU-TCS NPs	5-FU-TCS NPs from the co-administered system
Tmax	Hours	1	1
Cmax	µg/ml	56.51 ± 2.24	53.25 ± 4.61
AUC 0-t	µg/ml*Hour	1974.69 ± 248.37	1653.74 ± 137.02

Table 3.6. The number of phytotoxic values where the description of the pharmacokinetic values of the 5-FU-TCS NPs and 5-FU-TCS NPs had been respective to intravenous injection of Swiss Albino mice under the co-administered system which involved the time interval of 72hours.

In the same way, the individual sample intake(CRCTCS NPs alone) and other plus the system(combine 5-FU-TCS NPs and CRC-TCS NPs) had the highest plasma concentration(Cmax) of 18.00 + -3.54 10 -1 and 17.73 + -2.64 10 -1 respectively at 24 th hour. CRC single and coadministered time profile of systems plasma concentration showed time-related decrease. However, the plasma level of CRC in the NPs system was kept at the 3ug/ml levels compared with bare CRC (the highest plasma concentration rate was 100 + or -5.3 mg/ml that was obtained after an hour and was not obtained during the initial 6 hours).

Parameters	Units	CRC-TCS NPs	CRC-TCS NPs from the co-administered system
T_{max}	Hours	24	24
C_{max}	µg/ml	18 ± 3.54	17.73 ± 2.64
AUC_{0-t}	µg/ml*Hour	1046.37 ± 122.28	1023.29 ± 163.07

The pharmacokinetic values of the pharmacokinetic rates of the CR-TCS NPs and the CR- TCS NPs in the intravenous injection (following 72hours) of the Swiss Albino mice are presented in Table 3.7.

Its AUC0-t of 5- FU-TCS NPs, 5-FU- TCS NPs of the coadministration system is 1974.69 +248.37 5- FU-TCS and 5- FU- TCS respectively and is very high in comparison with the values of the AUC0 -t. This led to the entrapment effect of the 5-FU/CRC in the N, O-CMC NPs and in the TCS NPs to induce the enhancement effect on the 5-FU and CRC plasma concentration with time profile. The time profiles of plasma concentration of the systems were compared when administered co-administration with individual administration. Survey of the outcome of AUC 0 -t of single and the co administered system has been used to determine this. The difference between the co-administered and single one in the value of the AUC 0-t was not significant (Table 3.4, 3.5, 3.6, 3.7 and 3.8). These systems of nanoparticles of 5-FU and CRC have high AUC0-t values, thereby suggesting that the two drugs are more bioavailable and it arguably could not have been achieved in the case of uncoated drug solutions.

Therefore, the results of our experiments evidences indicated that the 5-FU-N, O-CMC NPs, 5-FUTCS NPs NP, CRC-N, O-CMC NPs and CRC-TCS NPs were able to survive in the blood the higher concentration to be able to conclude that it was able to be better preserved in blood. It is also noted further that Cmax of 5- F U and CRC also possess low values in the plasma where AUC is high in comparison with the bare drugs which are being used as control. This signifies that three of the discharged 5-FU and CRC were in the N, OCMC and TCS nanoparticles discharged into the blood in the deporting nanoparticles were progressively disintegrated (392). The nanomedicines under research enhanced bioavailability of 5-FU and CRC because the drugs in question were carried through the control delivery within the long duration of time. The pharmacokinetic activity of the nanoformulation of CRC and 5-FU is higher since the pharmaceutical takes a reasonable duration before being released on the blood following the carrier system. Our findings of enhanced bioactivity of CRC and 5-FU were producing positive tendencies to already existing literature.

It is a strong evidence that 5FU of 5-FU-N, O-CMC NPs and 5-FU-TCS NPs biodistribution is concentrated in the This could be due to the reason that 5-FU is a hydrophilic substance and thus accumulating more material in the kidney. This is attributable to the fact that the frequency of perfusion of the body organs is high and leads to the 5-FU remaining in the liver and the spleen.
Fig. 3.30C biodistribution of pattern of CRC of the CRC-N, O- CMC NPs (individual and co- administered system) also was similarly close to the biodistribution pattern of the CRC-N as in Fig. 3.30C. CRC could have been caused by the liver drug metabolism and liver elimination and renal clearance. Spleen location and the lung could be more correlated with the ingestion of the macrophages in such organs. It is possible that the filtration of pulmonary capillary bed and intravenous injection of the nanoparticles could be the cause why the CRC remains in the lungs. The traces are not numerous in the brain and it could be attributed to the fact that the hydrophobic CRC penetrates the barrier of blood brain. CRC retention in the heart may occur because of high results of heart perfusion.

3.12 Histology studies

The H and E staining was applied to the historic tissue sections of the treated mice organs and observed on the change on the histopathology and discussed at Table 3.9, Table 3.10 and Fig. 3.31-3.35(representative figure panel). Fig. 3.31H and E images were measured in the control samples as (A) saline treated and (B) combination of bare drugs treated animal (brain, heart, lungs, kidney, liver and spleen). The images of the organ stained with H and E were shown in Fig. 3.32and 3.33, respectively, the images of N, O-CMC system, respectively, and the mechanism was subjects to co administration system (CRC- N, O-CMC NPs, 5-FU-N-O CMC NPs. Fig. 3.34, and 3.35 showed the images of TCS system, respectively, CRC- TCS NPs and co administered one-CR.

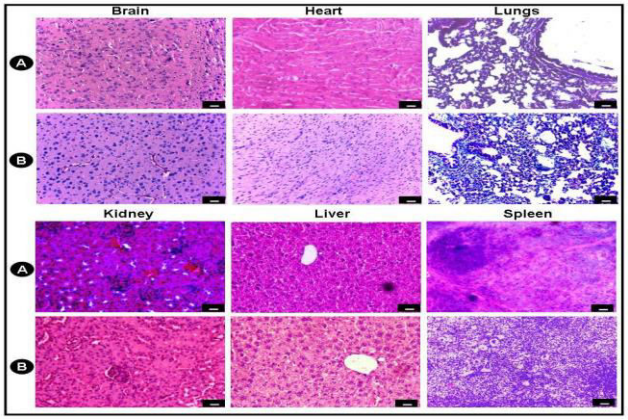

Figure 3.20. Represents the optical images of H and E stained control mice organs (brain, heart and lungs, kidney, liver and spleen) after 72 hours, where (A) saline, and (B) combination of bare drugs (scale bar represents 20 microns)(n=4).

In comparison with the controls, the CRC-treated (as in the case of CRC- N,O-CMC NPs and CRC-TCS NPs) organs didn't reveal any kind of pathological changes (brain, heart, lungs, kidney, liver and spleen), which proves the biocompatibility of the developed formulations. In all the selected tissues samples (kidney, liver and spleen), there is morphological deterioration of normal histological structures in 5-FU-NPs (5-FU-N, O-CMC NPs and 5-FU-TCS NPs) and combination of NPs (both N, O-CMC and TCS system) treated groups. In kidney, the renal glomeruli and tubules were reduced in size and these structures are replaced by fibrotic/necrotic tissues. Similarly, the hepatocytes in liver and lymphatic cells in spleen showed mild degenerative changes (deterioration of normal histological structures and are replaced by fibrotic tissues). Mild hyperemia is also visible in kidney, and spleen tissues indicating mild vascular congestion secondary to this tissue degeneration.

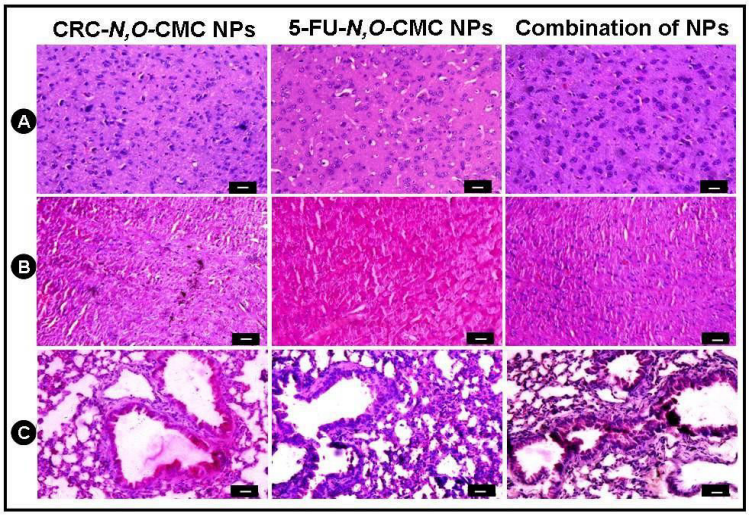

Figure 3.21. Represents the optical images of H and E stained mice organs; (A) brain, (B) heart, and (C) lungs after 72 hours of sample (CRC-N, O-CMC NPs, 5-FUN, O-CMC NPs and combination of NPs) administration (scale bar represents 20 microns)(n=4).

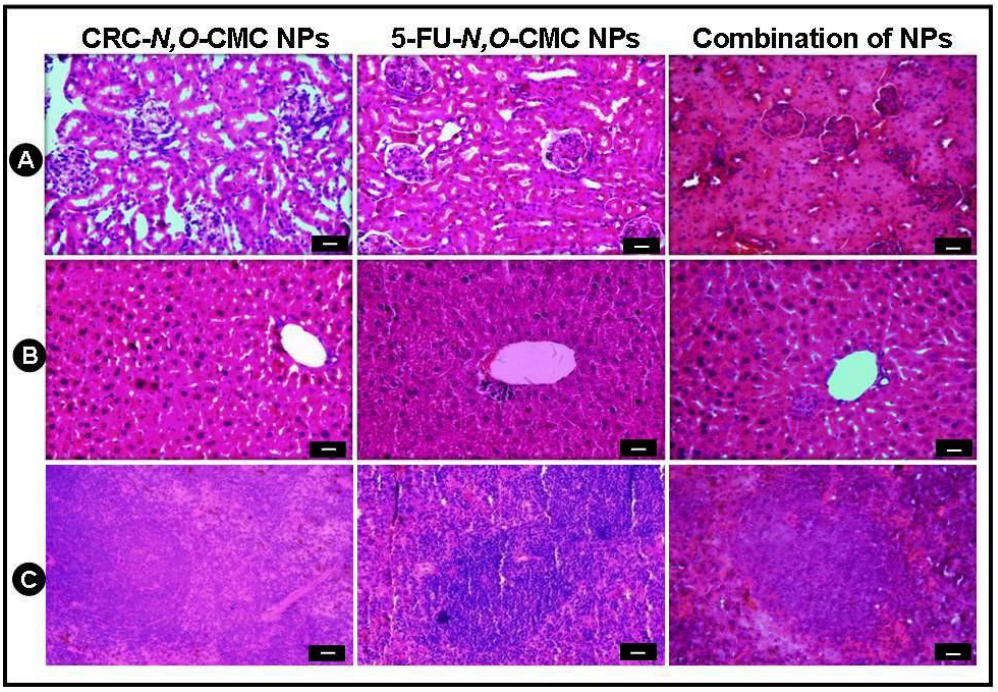

Figure 3.22. Represents the optical images of H and E stained mice organs, (A) kidney, (B) liver and (C) spleen after 72 hours of sample (CRC- N, O-CMC NPs, 5FU-N, O-CMC NPs and combination of NPs) administration (scale bar represents 20microns) (n=4).

Samples	Brain	Heart	Lungs	Kidney	Liver	Spleen
Saline	Normal	Normal	Normal	Normal	Normal	Normal
Combination of Bare Drugs	Normal	Normal	Normal	Normal	Normal	Normal
CRC-*N,O*-CMC NPs	Normal	Normal	Normal	Normal	Normal	Normal
5-FU-*N,O*-CMC NPs	Normal	Normal	Normal	Mild congestive and degenerative changes	Mild congestive and degenerative changes	Mild congestive and degenerative changes
Combination of 5-FU/CRC-*N,O*-CMC NPs	Normal	Normal	Normal	Mild congestive and degenerative changes	Mild congestive and degenerative changes	Mild congestive and degenerative changes

Table .3.8. Depicts the histopathological observation of mice organs after treating with saline, 5-FU-N,O-CMC NPs, CRC- N,O-CMC NPs, and the combination of 5FU- N,O-CMC NPs/CRC- N,O-CMC NPs along with the combination of bare drugs(as sample control) after 72 hours.

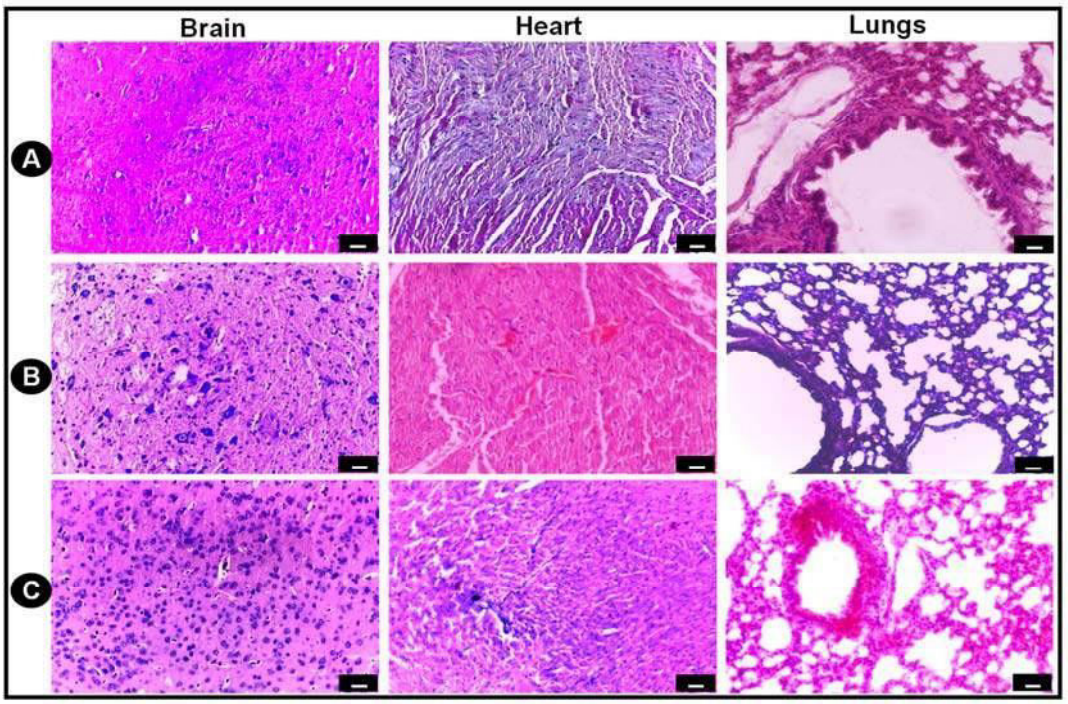

Figure 3.23. Represents the optical images of H and E stained mice organs; brain, heart and lungs after 72hours of sample (A: CRC-TCS NPs, B: 5-FU- TCS NPs and C: combination of NPs) administration (scale bar represents 20 microns) (n=4).

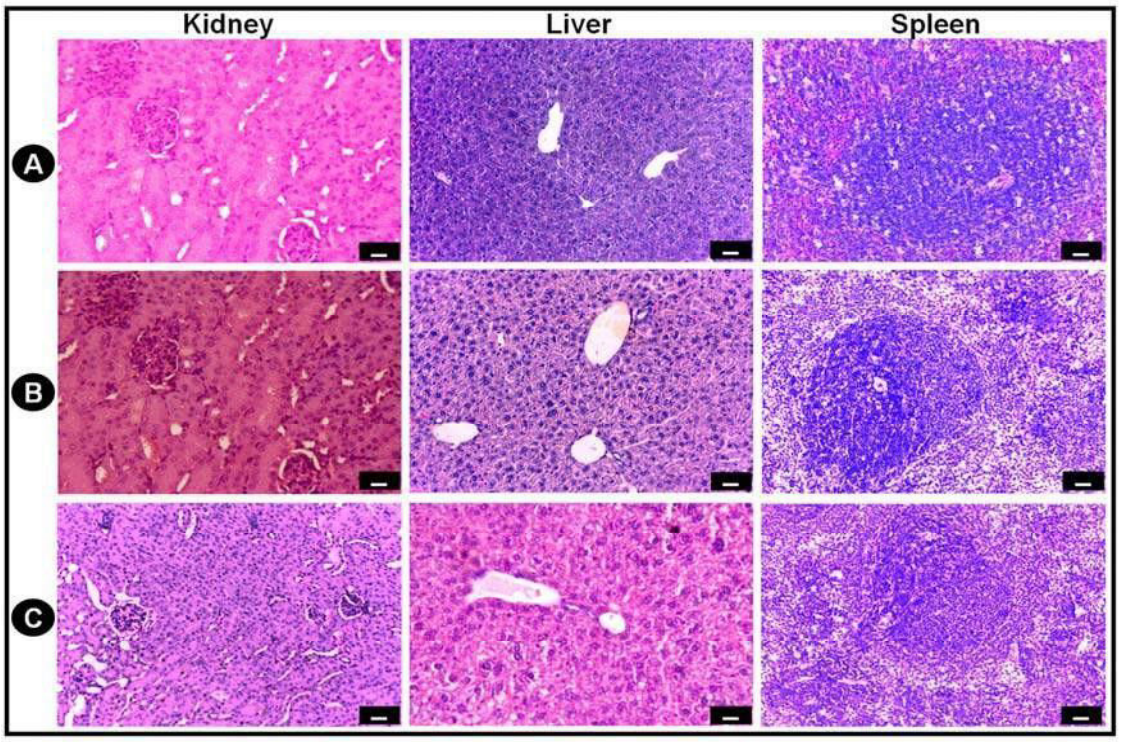

Figure 3.24. Represents the optical images of H and E stained mice organs; kidney, liver, and spleen after 72hours of sample (A: CRC- TCS NPs, B: 5-FU- TCS NPs and C: combination of NPs) administration (scale bar represents 20microns)(n=4).

Samples	Brain	Heart	Lungs	Kidney	Liver	Spleen
CRC-TCS NPs	Normal	Normal	Normal	Normal	Normal	Normal
5-FU-TCS NPs	Normal	Normal	Normal	Mild congestive and degenerative changes	Mild congestive and degenerative changes	Mild congestive and degenerative changes
Combination of 5-FU/CRC-TCS NPs	Normal	Normal	Normal	Mild congestive and degenerative changes	Mild congestive and degenerative changes	Mild congestive and degenerative changes

Table 3.9. Depicts the histopathological observation of mice organs after treating with saline, 5-FU-TCS NPs, CRC-TCS NPs, and the combination of 5-FU- TCS NPs/CRC- TCS NPs after 72 hours.

Thus the histopathological observation showed the absence of pathological changes in CRC treated systems. For the 5-FU system, we could see some congestive and degenerative changes. This can be lowered by reducing the concentration 5-FU containing nanoparticles in such a way that in cancer models, 5-FU-NPs could produce synergistic anticancer effects with CRC NPs.

CONLCUSION

One of the promising curative approaches to colorectal cancer (CRC) is the use of probiotics-impregnated curcumin nanoparticles that are stuffed with curcumin. Entrapping curcumin in chitosan-based nanoparticles increased the solubility, solution stability, as well as bioavailability of the compound greatly since it is more viable when it comes to the treatment of CRC. The synergy between the two in increasing the cytotoxicity and cell death by the splenic effect of the curcumin-loaded nanoparticles in vitro of the HT-29 CRC cells on tumor microenvironment immunomodulatory action is also typical of the probiotics (in which, immunomodulatory action is widespread). Nanoparticle preparations whereby the curcumin releases were attained were regulated and sustained the ones that led to the tumor cell growth inhibitory and tumor cell-icterating induction. Besides this, the probiotics enhanced the stability and bioavailability of curcumin, and this resulted in formation of the more successful cancer treatment regimen due to the improved systemic retention and bioavailability of curcumin and reduced the off-target toxicity.Research on the in vivo pharmacokinetics and biodistribution demonstrated that the nanoparticle preparations enhanced the systemic retention and bioavailability of curcumin and minimized the off-target toxicity. More likely, it was the trapping of curcumin as a nanoparticle in probiotics, which led to further enhancement of the therapeutic activity and minimization of the adverse effects that is of utmost importance to enhance the quality of life related to the patient receiving the therapeutic intervention. These facts indicate that probiotics could be replaced or administered among other conventional chemotherapy which could be more specific and effective in the convergence of the curcumin-loaded chitosan nanoparticles. The controlled drug release profile of drug delivery is high and this means that this kind of drug delivery has a high potential in the treatment regimen of the CRC with lower systemic toxicity. This combination therapy still could have been enhanced better and several clinical trials would have been conducted on this combination therapy in future studies which would have resulted to the development of more effective therapy to CRC, and indirectly to other cancers.

REFERENCES

1. Mogadem, A., El-Kady, H., Eskandrani, A., Abou-Taleb, B. A., Salah, S., Samir, N., ... & Elwakil, B. H. (2025). Probiotic bacteria combined with curcumin-loaded chitosan nanoparticles as a promising anti-colorectal cancer agent. *Journal of Drug Delivery Science and Technology*, 107415.
2. Saberpour, M., Maqsoodi, R., & Bakhshi, B. (2025). Anti-cancer properties of chitosan/Lactobacillus acidophilus secretome nanoparticle on signaling pathways of colorectal cancer in colon adenocarcinoma (Caco-2) cell line. *BMC cancer*, *25*(1), 983.
3. Gunasangkaran, G., Ravi, A. K., Arumugam, V. A., & Muthukrishnan, S. (2022). Preparation, characterization, and anticancer efficacy of chitosan, chitosan encapsulated piperine and probiotics (Lactobacillus plantarum (MTCC-1407), and Lactobacillus rhamnosus (MTCC-1423) nanoparticles. *BioNanoScience*, *12*(2), 527-539.
4. Maqsoodi, R., Saberpour, M., Bakhshi, B., & Fallah, F. (2025). Effect of chitosan nanoparticles conjugated with the cell free supernatant of Bifidobacterium bifidum on the expression of genes related to colorectal cancer in colon adenocarcinoma (Caco-2) cell line. *BMC gastroenterology*, *25*(1), 394.
5. Jadid, M. F. S., Jafari-Gharabaghlou, D., Bahrami, M. K., Bonabi, E., & Zarghami, N. (2023). Enhanced anti-cancer effect of curcumin loaded-niosomal nanoparticles in combination with heat-killed Saccharomyces cerevisiae against human colon cancer cells. *Journal of Drug Delivery Science and Technology*, *80*, 104167.
6. Derakhshan-Sefidi, M., Bakhshi, B., & Rasekhi, A. (2024). Vibriocidal efficacy of Bifidobacterium bifidum and Lactobacillus acidophilus cell-free supernatants encapsulated in chitosan nanoparticles against multi-drug resistant Vibrio cholerae O1 El Tor. *BMC Infectious Diseases*, *24*(1), 905.

7. Firouzi Amandi, A., Jokar, E., Eslami, M., Dadashpour, M., Rezaie, M., Yazdani, Y., & Nejati, B. (2023). Enhanced anti-cancer effect of artemisinin-and curcumin-loaded niosomal nanoparticles against human colon cancer cells. *Medical Oncology*, *40*(6), 170.
8. Firouzi Amandi, A., Jokar, E., Eslami, M., Dadashpour, M., Rezaie, M., Yazdani, Y., & Nejati, B. (2023). Enhanced anti-cancer effect of artemisinin-and curcumin-loaded niosomal nanoparticles against human colon cancer cells. *Medical Oncology*, *40*(6), 170.
9. Kedar, P., Bhattacharya, S., Sakore, P., & Prajapati, B. G. (2025). Advanced Targeted Therapy for Colorectal Cancer with Lipid Nanoparticles. *Current Medicinal Chemistry*.
10. Choukaife, H., Seyam, S., Alallam, B., Doolaanea, A. A., & Alfatama, M. (2022). Current advances in chitosan nanoparticles based oral drug delivery for colorectal cancer treatment. *International journal of nanomedicine*, 3933-3966.
11. Li, S., Lu, S., Xiong, J., Chen, L., Lin, Y., Chen, X., ... & Yang, X. (2025). Hydroxyethyl starch-curcumin nanoparticles ameliorate DSS-induced ulcerative colitis in mice via synergistic TLR4/NF-κB suppression, Nrf2 activation, intestinal barrier restoration, and gut microbiota modulation. *Frontiers in Pharmacology*, *16*, 1610711.
12. Zhang, R., Zhang, W., Zhang, Q., Wang, L., Yang, F., Sun, W., ... & Wang, M. (2024). Curcumin-Modified Selenium Nanoparticles Improve S180 Tumour Therapy in Mice by Regulating the Gut Microbiota and Chemotherapy. *International Journal of Nanomedicine*, 13653-13669.
13. Zhang, R., Zhang, W., Zhang, Q., Wang, L., Yang, F., Sun, W., ... & Wang, M. (2024). Curcumin-Modified Selenium Nanoparticles Improve S180 Tumour Therapy in Mice by Regulating the Gut Microbiota and Chemotherapy. *International Journal of Nanomedicine*, 13653-13669.
14. Feng, T., Paul, B., & Chen, W. (2025). Synergistic effects of co-delivery bioactive compounds using polymeric-based nanoparticles for biological activities: Recent trends. *Food Quality and Safety*, fyaf061.
15. Muppala, S., & Konduru, S. K. P. (2020). Crucial Role of Curcumin in Gut Microbiota Associated with GI Cancers. In *Phytochemicals Targeting Tumor Microenvironment in Gastrointestinal Cancers* (pp. 109-117). Cham: Springer International Publishing.
16. Re, F., Pelucchi, S., Pettini, F., Prantera, A., Troisi, F., Mahmoud, R. M. A., ... & Barisani, D. (2025). Emerging nanocarrier systems for the enhanced delivery of active pharmaceutical ingredients to the intestine. *Nanomedicine*, 1-24.
17. Vieira, I. R. S., & Conte-Junior, C. A. (2024). Nano-delivery systems for food bioactive compounds in cancer: Prevention, therapy, and clinical applications. *Critical Reviews in Food Science and Nutrition*, *64*(2), 381-406.
18. Hasan, A., Rani, S., & Hussain, A. (2025). Harnessing Engineered Probiotics for Gastrointestinal Diseases Therapy. In *Cell Membrane Engineering for Advancing Cell-Based and Nanotechnology-Based Therapies* (pp. 275-302). Cham: Springer Nature Switzerland.
19. Tang, Y., Liu, W., Zhang, J., Juan, B., Zhu, Y., Zhu, L., ... & He, Y. (2025). Advances in Intestinal-Targeted Release of Phenolic Compounds. *Nutrients*, *17*(16), 2598.
20. Pathomthongtaweechai, N., & Muanprasat, C. (2021). Potential applications of chitosan-based nanomaterials to surpass the gastrointestinal physiological obstacles and enhance the intestinal drug absorption. *Pharmaceutics*, *13*(6), 887.
21. Ahmed, H. H., Kotob, S. E., Abd-Rabou, A. A., Aglan, H. A., Elmegeed, G. A., & Mohawed, O. A. (2021). Pre-clinical evidence for the anti-obesity potential of quercetin and curcumin loaded chitosan/PEG blended PLGA nanoparticles. *Biomedical and Pharmacology Journal*, *14*(4), 1731-1759.
22. Archana 1, & Deshmukh, R. (2024). Recent trends in nanotechnological approach in targeting selenium nanoparticles for the treatment of colorectal cancer. *Nanoscience & Nanotechnology-Asia*.